Physics-based Decoding Improves Magnetic Resonance Fingerprinting*

Juyeon Heo*[1], Pingfan Song*[1], Weiyang Liu[1], and Adrian Weller[1,2]

[1] University of Cambridge
[2] The Alan Turing Institute
{jh2324,ps898,wl396,aw665}@cam.ac.uk

Abstract. Magnetic Resonance Fingerprinting (MRF) is a promising approach for fast Quantitative Magnetic Resonance Imaging (QMRI). However, existing MRF methods suffer from slow imaging speeds and poor generalization performance on radio frequency pulse sequences generated in various scenarios. To address these issues, we propose a novel MRI physics-informed regularization for MRF. The proposed approach adopts a supervised encoder-decoder framework, where the encoder performs the main task, i.e. predicting the target tissue properties from input magnetic responses, and the decoder servers as a regularization via reconstructing the inputs from the estimated tissue properties using a Bloch-equation based MRF physics model. The physics-based decoder improves the generalization performance and uniform stability by a considerable margin in practical out-of-distribution settings. Extensive experiments verified the effectiveness of the proposed approach and achieved state-of-the-art performance on tissue property estimation.

Keywords: Magnetic Resonance Fingerprinting · Deep Neural Network · Physics-informed learning · Generalizability · Bloch equations

1 Introduction

Quantitative Magnetic Resonance Imaging (QMRI) is used to identify tissue's intrinsic physical properties, including the spin-lattice magnetic relaxation time (T1), and the spin–spin magnetic relaxation time (T2) [23, 23]. Compared to conventional weighted (qualitative) MRI that focuses on tissue's contrast of brightness and darkness, QMRI reveals tissue's intrinsic properties with quantitative values and associated physical interpretations. Since different tissues are characterized by their distinct properties values, QMRI shows great potential to reduce subjectivity, with advantages in many areas including diagnosis, tissue characterization, investigation of disease pathologies, personalized medical treatment, and therapeutic assessment [1, 10, 28].

* Supported by Turing AI Fellowship under EPSRC grant EP/V025279/1, by the Leverhulme Trust via CFI, and by Northern Ireland High Performance Computing (NI-HPC) service funded by EPSRC(EP/T022175). Co-first authors: J. H. & P. S.; Corresponding author: P. S. (ps898@cam.ac.uk)

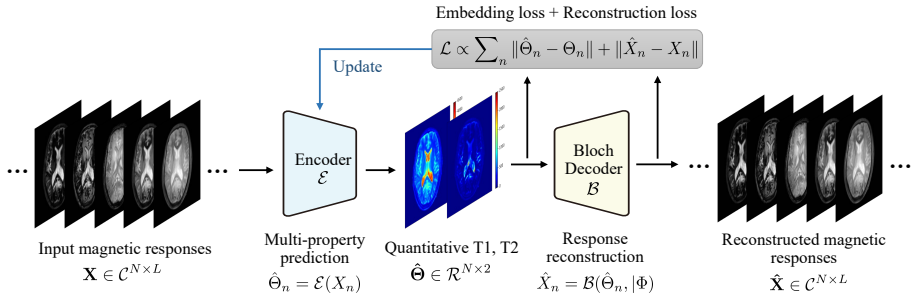

Fig. 1: BlochNet adopts a supervised encoder-decoder framework where the encoder solves an inverse problem that predicts tissue properties from input magnetic responses while the decoder leverages a Bloch equations-based MRI physics model to reconstruct the input responses from the estimated tissue properties. Such a design helps the encoder capture generalizable mapping effectively with the aid of physics-based feedback from the Bloch decoder.

Despite various benefits, most QMRI approaches suffer from slow imaging speeds, and usually provide only a single intrinsic property at a time (*e.g.*, quantification of T1 alone, followed by T2 alone), resulting in low throughput. Magnetic Resonance Fingerprinting (MRF) provides an alternative QMRI framework to achieve multi-property quantification simultaneously [16]. Given a pseudo-random radio frequency (RF) pulse sequence, a distinct magnetic response, *i.e.*, fingerprint / signature, from each specific tissue is observed and then used to predict the target intrinsic tissue properties, *e.g.*, T1 and T2 values. Therefore, multi-property quantification boils down to an inverse problem that aims to infer underlying tissue properties from the observed magnetic responses.

In this work, we propose an MRI physics-regularized deep learning model for fast and robust MRF, called *BlochNet* as shown in Fig. 1. BlochNet adopts a supervised encoder-decoder framework where the encoder network solves the primary inverse problem that predicts tissue properties from input magnetic responses, while the decoder acts as a regularizer that guides the training of the encoder. In particular, the decoder leverages a Bloch equations-based MRI physics model to reconstruct the input responses from the estimated tissue properties, and compares the reconstructed inputs with the original input to provide an additional loss for the regularization purpose.

The rationale underlying the design is that domain knowledge such as well-founded physics principles bring additional useful constraints that can effectively reduce the solution space of an inverse problem. This contributes to an optimized solution, in particular, for an (ill-posed) inverse problem [11, 12, 15, 18]. Our results verify that the proposed approach exhibits improved robustness and generalization performance in both synthetic and real MRF data in two different out-of-distribution (OOD) settings. The major contributions include:

– The proposed BlochNet incorporates an MRI physics model to the decoding mechanism, which plays a role to regularize the training of the encoder. We

expect that such a physics-based design can provide useful training signals for the encoder to better solve the MRF problems.
- We improve the efficiency of the implementation of the Bloch equations, which reduce the computation overhead such that the MRI physics-based decoding model can be used directly as a differentiable module and trained end-to-end in neural networks (*e.g.*, the decoder in BlochNet).
- Compared to existing methods, BlochNet shows consistently better generalization performance across synthetic, phantom and real MRF data, and across different types of RF pulse sequences.

2 Background and Related works

Since tissue properties lead to magnetic responses according to the MRI dynamics, quantifying tissue's properties via QMRI/MRF is a typical inverse problem, also an anti-causal task. The core idea of MRF is based on the fact that for each specific tissue, a pseudo-random pulse sequence leads to a unique magnetic response (*i.e.*, magnetization along the temporal dimension) which can serve as an identifiable signal signature, analogous to a "fingerprint" for the corresponding tissue. Once the unique identifiable magnetic responses are obtained, the estimation of tissue properties reduces to a pattern recognition problem.

Various approaches have been developed to solve the MRF problem, using either model-based techniques, *e.g.*, dictionary matching (DM), compressive sensing, or learning-based / data-driven techniques.

Model-based approaches. In the original MRF work [16], this task is approached via dictionary matching (DM) which finds the best matching entry in a pre-computed dictionary for each inquiry magnetic response. Accordingly, the best matching dictionary entry leads to multiple tissue properties directly via a look-up-table (LUT) operation. To alleviate the extensive computation overhead and storage burden, a number of model-based MRF approaches [7, 20, 25] were proposed to incorporate additional useful priors, e.g. sparsity, low rank, in order to improve reconstruction performance as well as reduce computational complexity.

Learning-based approaches. To address some shortcomings of model-based methods, learning-based approaches have been proposed for fast MRF by replacing the dictionary with a compact neural network. In particular, motivated by the success of deep learning in a number of tasks, there is an emerging trend [5, 6, 9, 24] that suggests to use a trained neural network as a substitute for the MRF dictionary and LUT, so that the time-consuming dictionary matching operation can be avoided and replaced by an efficient inference through a trained network. However, despite the good performance delivered by neural networks, most of the learning-based methods were designed without taking into account the MRI physics underlying the imaging process, and may inevitably suffer from some limitations, such as degraded robustness and generalizability.

Physics-informed learning. Another highly related line of research is model-based learning [21, 22] which provides a promising path to integrate domain knowledge with learned priors, thereby fusing the benefits of model-based

methods with learning-based methods. Typical examples include algorithm unrolling [21], physics-informed neural networks (PINNs) [22], and other variants. Incorporating physics priors into the neural network design and training has demonstrated benefits in a broad range of applications [3, 17], in particular for medical imaging [5, 28, 29]. In a similar spirit, we aim to incorporate the physics model that describes the MRI dynamics into learning-based MRF approaches so that the learned model can demonstrate improved data efficiency, robustness and generalization. Note that, in contrast to standard PINNs which are used to solve a PDE, our task is to solve an inverse PDE. Furthermore, we propose to leverage the PDE as a regularization. (More related work and comparisons are provided in the Appendix.)

3 Problem Formulation and Method

3.1 BlochNet: Regularized Networks by Physics-based Decoding

The proposed BlochNet adopts a supervised encoder-decoder framework where the encoder solves the primary inverse problem that predicts tissue properties from input magnetic responses, while the decoder solves an auxiliary task that reconstructs the inputs from the estimated tissue properties using the Bloch equations-based MRI physics model. We highlight that a sophisticated MRI physics model is tailored and exploited as the decoder. The rationale behind such a design lies in the fact that the data generation mechanism represented by MRI physics is a useful constraint that can effectively reduce the solution space of the inverse problem. Therefore, the physics-based decoder will act as a strong regularizer that can provide informative feedback and contribute to the training of a better encoder. We expect the physics prior can introduce a better and generalizable inductive bias to the encoder. Similar ideas have been explored in some other domains [11, 12, 18].

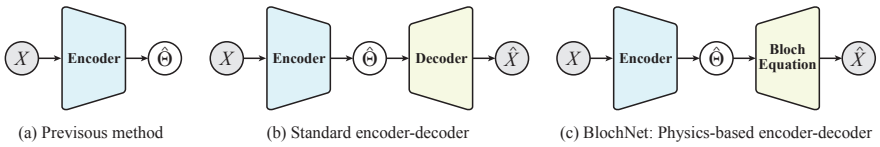

Fig. 2: Two baseline methods and our BlochNet. BlochNet exploits physics-based decoder for helping the encoder learn generalizable representation.

Specifically, in the proposed approach, the encoder uses a three-layer fully connected neural network to address the inverse problem that predicts T1, T2 tissue properties from input magnetic responses. Given an enquiry magnetic response $X_n \in \mathbb{C}^L$ for the n-th voxel where L denotes the length of each magnetic response, e.g. L = 1000 in our experiments, the encoder $\mathcal{E}$ outputs predicted

tissue properties $\hat{\Theta}_n = \{\hat{T1}_n, \hat{T2}_n\} \in \mathbb{R}^p$ where $p = 2$ denotes the number of tissue properties to be predicted.

$$\hat{\Theta}_n = \mathcal{E}(X_n) \quad \forall n \in 1, \ldots, N$$

Note that, the estimation of tissue properties Θ from magnetic responses X requires long enough sequences $L > p$ to create identifiable signal evolutions that distinguish different tissues. Hence, this operation nonlinearly maps the magnetic responses from a high-dimensional manifold to a low-dimensional manifold.

In contrast, the decoder reconstructs the input magnetic responses from the estimated tissue properties $\hat{\Theta}_n$ by solving the Bloch equations [2] using our fast extended phase graph (EPG) implementation, given RF pulse sequence settings $\Phi = \{FA, TR, TE\}$ which consists of flip angles $FA \in \mathbb{C}^L$, repetition times $TR \in \mathbb{R}^L$ and echo times $TE \in \mathbb{R}^L$ across L time points.

$$\hat{X}_n = \mathcal{B}(\hat{\Theta}_n | \Phi) \quad \forall n \in 1, \ldots, N$$

where $\mathcal{B}$ denotes the decoder based on Bloch equations:

$$\frac{d\vec{M}}{dt} = \vec{M} \times \gamma \vec{B} - \begin{bmatrix} M_x/T2 \\ M_y/T2 \\ (M_z - M_0)/T1 \end{bmatrix}$$

where $\vec{M} = [M_x, M_y, M_z]^\top$ denotes the magnetization vector. $\vec{M}_0$ denotes the equilibrium magnetization; $\vec{B}$ denotes the magnetic field; and γ denotes the gyromagnetic ratio. (More details of Bloch equations are provided in the Appendix.)

3.2 Fast EPG for solving Bloch equations

Since there is no general analytic solution to the Bloch equations, numerical solutions such as EPG formalism are often adopted. However, a limitation of the released EPG implementation [26] is its slow computation speed in solving the Bloch equations. To circumvent this, recurrent neural networks [14] and generative adversarial networks [27] have been applied as surrogates for the Bloch equation. However, these surrogate models require a lot of training data and may generate inaccurate magnetic responses on unseen tissue properties and RF pulse settings due to complex physics dynamics and potential overfitting risks.

Instead, we adapt the EPG implementation [26] to achieve a much more efficient implementation, making it practical to use the exact MRI physics model as a decoder in the training procedure. Specifically, the adaptations involve incorporating the PyTorch jit package for efficient parallelization, using batch-wise computation for the 3 Bloch stages (including nutation+forced precession, rotation, and relaxation in Fourier domain), and handling complex values in Pytorch efficiently. The improvement leads to 500 times faster generation of magnetic responses for 1,000 sequences on CPU, making repeated EPG computations feasible during training.[3] (More details can be found in the Appendix.)

[3] Our code, including the fast and end-to-end solvable EPG-Bloch code, is released on our GitHub repository at https://github.com/rmrisforbidden/CauMedical.git.

3.3 Loss function

The loss function consists of two parts: the mean squared error (MSE) between the ground truth and the predicted tissue properties, referred to as embedding loss, and the MSE between the input and the reconstructed signatures, referred to as reconstruction loss,

$$\mathcal{L} = \frac{1}{N}\sum_{n=1}^{N}\left(\frac{1}{2}\|\hat{\Theta}_n - \Theta_n\|_2^2 + \frac{1}{2}\|\hat{X}_n - X_n\|_2^2\right).$$

4 Experiment results

In this section, we perform an evaluation of the proposed method and conduct a comparison with other state-of-the-art MRF methods. We evaluate the generalization performance of all models across different data distributions and different RF pulse sequences. The evaluation metric is the MSE in log-scale, and therefore, the unit is the squared millisecond in log-scale. For our model, we use 3-layer encoder-decoder with varying hidden units, Adam optimizer (lr=1e-3), and maximum epochs of 100 with early stopping based on the validation set on GTX 1080 Ti. We performed ten independent trials, the results of which are presented in Table 1 and 2. The associated standard deviations are provided in the Appendix.

4.1 Data settings and baseline methods

We exploit three types of data including synthetic data, phantom MRI data, and anatomical MRI data. In particular, synthetic data (around 80,000 samples) is used for training, while phantom data (85,645 samples) and anatomical data (7,499 samples) is for evaluation. More details about the three datasets are provided in the Appendix. We compare our approach with 6 representative state-of-the-art MRF methods, including dictionary matching (DM) [16], Fully-connected deep neural network (FC) [6], Hybrid deep learning (HYDRA) [24] as well as two auto-encoder methods with RNN encoder and RNN decoder(RNN-RNN) and FC encoder and FC decoder(FC-FC), respectively.

	Dictionary Matching	FC	RNN	HYDRA	Autoencoder (FC-FC)	Autoencoder (RNN-RNN)	BlochNet (FC-Bloch)
Phantom data	18.6656	0.0634	0.0457	0.1604	0.0529	0.0508	**0.0311**
Anatomical data	19.4886	0.0795	0.0574	0.3109	0.0771	0.0987	**0.0647**

Table 1: Generalization performance across **different data distributions**: synthetic data for training while phantom and anatomical data for testing.

4.2 Experiments of evaluating generalization performance

We evaluate the generalization performance of various models on two types of experiment settings: 1) across different data distributions, including synthetic, phantom and anatomical MRF data; 2) across different RF pulse sequences with different flip angles. In addition, a series of ablation studies were conducted via comparison with other methods that use different types of decoders, as shown in Table 1 and Table 2, for example, comparing BlochNet (using a physics-based decoder) with FC (using no decoder) and FC-FC (using a learned decoder) to show the effect of the encoder and the effect of MRI physics.

Generalization across different data distributions Due to limited anatomical data with ground truth T1, T2 values, it is common practice to use a large amount of synthetic data to train models to avoid potential overfitting, and then perform validation on anatomical data [4, 7, 8, 13, 19, 20, 24, 25]. Following the same routine, we perform model training on synthetic MRF data, followed by model testing on phantom and anatomical data, in order to evaluate the generalization performance of trained models across different data distributions.

Table 1 includes the mean squared error (MSE) between the ground truth and predicted tissue properties for seven approaches on phantom and anatomical data (in log-scale). As shown in the table, the dictionary-matching approach gave the worst performance, because the pre-computed dictionary and LUT did not cover the OOD data samples that could be quite different from the already contained dictionary entries. Interestingly, the results show that the reconstruction loss provides benefits to between-data generalization for autoencoder models(FC-FC or RNN-RNN), in comparison with non-autoencoder models(FC or RNN), respectively, on both phantom and anatomical MRF data. Furthermore, our BlochNet outperforms all other models, indicating that reconstruction loss from the physics-based decoder has the best regularization effect that contributes to improved encoder training.

Figure 3 shows the predicted tissue properties using various models on anatomical MRF data. Each individual model shows different prediction characteristics. Specifically, HYDRA suffers from a higher loss at the rim region of the brain, and leads to larger errors than other models. Autoencoder(FC-FC) model demonstrates better prediction of T2 values than the non-autoencoder(FC) model. The proposed BlochNet outperforms other models with the least prediction error and most stable performance across the whole range of both T1 and T2 values.

Generalization across different RF pulse sequences In this experiment, we perform model training on one RF pulse sequence and evaluate the trained models on a different RF pulse sequence. Specifically, we adopted 3 different RF pulse sequences, including FISP [16], Spline5 [14], Spline11Noisy [14] with their flip angles shown in Figure 1 in the Appendix. More details are provided in Appendix. FISP is used exclusively in the testing stage, while Spline5 and Spline11Noisy are used exclusively in the training stage. Under such settings, the performance of our BlochNet and other six models is compared in Table 2.

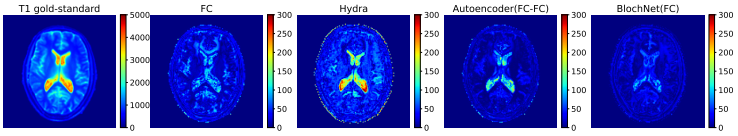

(a) Gold-standard T1 and prediction errors

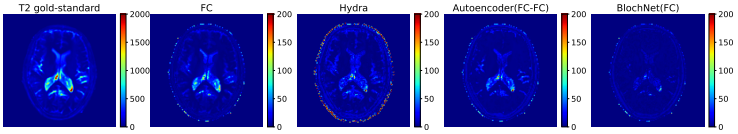

(b) Gold-standard T2 and prediction errors

Fig. 3: Generalization across **different data distributions**: data in training is synthetic while in testing is anatomical MRI for four different models.

	Dictionary Matching	FC	RNN	HYDRA	Autoencoder (FC-FC)	Autoencoder (RNN-RNN)	BlochNet (FC-Bloch)
Phantom data	27.1956	0.8349	0.7960	0.3599	0.6968	0.6269	**0.1543**
Anatomical data	16.6150	0.7331	1.0674	0.6961	0.4021	0.9455	**0.2766**

Table 2: Generalization performance across **different RF pulse sequences**: Spline5 and SplineNoisy11 in training, FISP in testing.

In spite of degraded performance for all models under different train and test RF pulse sequences, the results clearly show the advantage of autoencoder (FC-FC or RNN-RNN) models over non-autoencoder models(FC or RNN), which confirms the benefits of incorporating a decoder to derive the reconstruction loss as additional regularization. Furthermore, the proposed BlochNet demonstrates significant gains over competing methods in such challenging cases on both phantom and anatomical MRF data.

In Figure 4, FC model (left) makes poor predictions on both T1 and T2 values with high variance, because it cannot infer tissue properties from input signatures generated from different combinations of T1 and T2 values. Autoencoder(FC-FC) model (third column) shows more aligned and better inferences with lower variance, but still has high deviation between predicted and gold-standard values. In comparison, our BlochNet outputs predictions that are closest to the gold-standard with the lowest error. This confirms the benefits of our physics-based decoder that guides the encoder to learn the underlying anti-causal mechanism effectively.

5 Discussion

We present statistical significance tests on 10 trials for pairwise group comparisons using Tukey HSD test after the Normality Test and repeated ANOVA. For results in Table 1, corresponding to setting 1 (a relatively easy problem as the RF pulses used in training and testing are the same), our method is not always statistically better to every compared method, since all baseline methods can

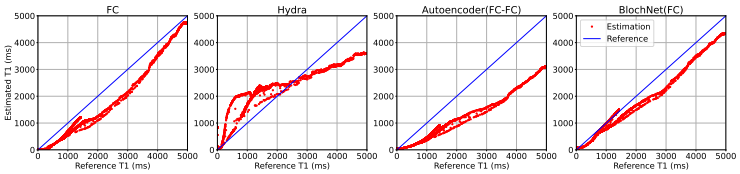

(a) T1 gold standard and predicted values.

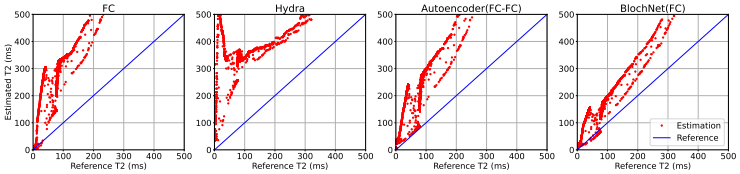

(b) T2 gold standard and predicted values.

Fig. 4: Comparison of the generalization performance across **different RF pulse sequences**. Blue line: gold-standard. Red dots: predicted values for T1 and T2.

perform reasonably well. However, in setting 2, a much more challenging OOD setting where the RF pulses used in testing are different from those used in training and therefore can lead to different magnetic responses, our method is always statistically better (p-value < 0.001) than compared methods according to the results in Table 2. This demonstrates the robustness and generalizability of our method. As far as we are concerned, no existing approaches achieved satisfactory results in such an OOD case. While there is still ample room for improvement across all the methods, our approach took a critical step forward by incorporating physics knowledge. (More details can be found in the Appendix.)

6 Conclusion

We propose BlochNet, a novel MRI physics-informed learning model, which consistently outperforms competing methods with better robustness and generalizability in MRF problems. In future work, we will consider k-space subsampling and incorporating spatial information for faster and more efficient QMRI/MRF.

Bibliography

[1] Bipin Mehta, B., Coppo, S., Frances McGivney, D., Ian Hamilton, J., Chen, Y., Jiang, Y., Ma, D., Seiberlich, N., Gulani, V., Alan Griswold, M.: Magnetic resonance fingerprinting: a technical review. Magnetic resonance in medicine **81**(1), 25–46 (2019)

[2] Bloch, F.: Nuclear induction. Physical review **70**(7-8), 460 (1946)

[3] Cai, S., Wang, Z., Wang, S., Perdikaris, P., Karniadakis, G.E.: Physics-informed neural networks for heat transfer problems. Journal of Heat Transfer **143**(6) (2021)

[4] Cao, X., Liao, C., Wang, Z., Chen, Y., Ye, H., He, H., Zhong, J.: Robust sliding-window reconstruction for accelerating the acquisition of mr fingerprinting. Magnetic resonance in medicine **78**(4), 1579–1588 (2017)

[5] Chen, D., Davies, M.E., Golbabaee, M.: Deep unrolling for magnetic resonance fingerprinting. In: 2022 IEEE 19th International Symposium on Biomedical Imaging (ISBI). pp. 1–4. IEEE (2022)

[6] Cohen, O., Zhu, B., Rosen, M.S.: MR fingerprinting deep reconstruction network (drone). Magnetic resonance in medicine **80**(3), 885–894 (2018)

[7] Davies, M., Puy, G., Vandergheynst, P., Wiaux, Y.: A compressed sensing framework for magnetic resonance fingerprinting. SIAM Journal on Imaging Sciences **7**(4), 2623–2656 (2014)

[8] Golbabaee, M., Buonincontri, G., Pirkl, C.M., Menzel, M.I., Menze, B.H., Davies, M., Gómez, P.A.: Compressive mri quantification using convex spatiotemporal priors and deep encoder-decoder networks. Medical Image Analysis **69**, 101945 (2021)

[9] Hamilton, J.I., Currey, D., Rajagopalan, S., Seiberlich, N.: Deep learning reconstruction for cardiac magnetic resonance fingerprinting t1 and t2 mapping. Magnetic Resonance in Medicine **85**(4), 2127–2135 (2021)

[10] Keil, V.C., Bakoeva, S.P., Jurcoane, A., Doneva, M., Amthor, T., Koken, P., Mädler, B., Lüchters, G., Block, W., Wüllner, U., et al.: A pilot study of magnetic resonance fingerprinting in parkinson's disease. NMR in Biomedicine **33**(11), e4389 (2020)

[11] Kilbertus, N., Parascandolo, G., Schölkopf, B.: Generalization in anti-causal learning. arXiv preprint arXiv:1812.00524 (2018)

[12] Le, L., Patterson, A., White, M.: Supervised autoencoders: Improving generalization performance with unsupervised regularizers. Advances in neural information processing systems **31** (2018)

[13] Liao, C., Bilgic, B., Manhard, M.K., Zhao, B., Cao, X., Zhong, J., Wald, L.L., Setsompop, K.: 3d mr fingerprinting with accelerated stack-of-spirals and hybrid sliding-window and grappa reconstruction. Neuroimage **162**, 13–22 (2017)

[14] Liu, H., van der Heide, O., van den Berg, C.A., Sbrizzi, A.: Fast and accurate modeling of transient-state, gradient-spoiled sequences by recurrent neural networks. NMR in Biomedicine **34**(7), e4527 (2021)

[15] Liu, W., Liu, Z., Paull, L., Weller, A., Schölkopf, B.: Structural causal 3d reconstruction. In: Proc. Eur. Conf. Comput. Vision (2022)
[16] Ma, D., Gulani, V., Seiberlich, N., Liu, K., Sunshine, J.L., Duerk, J.L., Griswold, M.A.: Magnetic resonance fingerprinting. Nature **495**(7440), 187 (2013)
[17] Mao, Z., Jagtap, A.D., Karniadakis, G.E.: Physics-informed neural networks for high-speed flows. Computer Methods in Applied Mechanics and Engineering **360**, 112789 (2020)
[18] Maurer, A., Pontil, M., Romera-Paredes, B.: The benefit of multitask representation learning. Journal of Machine Learning Research **17**(81), 1–32 (2016)
[19] Mazor, G., Weizman, L., Tal, A., Eldar, Y.C.: Low rank magnetic resonance fingerprinting. In: Engineering in Medicine and Biology Society (EMBC), 2016 IEEE 38th Annual International Conference of the. pp. 439–442. IEEE (2016)
[20] Mazor, G., Weizman, L., Tal, A., Eldar, Y.C.: Low-rank magnetic resonance fingerprinting. Medical physics **45**(9), 4066–4084 (2018)
[21] Monga, V., Li, Y., Eldar, Y.C.: Algorithm unrolling: Interpretable, efficient deep learning for signal and image processing. IEEE Signal Processing Magazine **38**(2), 18–44 (2021)
[22] Raissi, M., Perdikaris, P., Karniadakis, G.E.: Physics-informed neural networks: A deep learning framework for solving forward and inverse problems involving nonlinear partial differential equations. Journal of Computational physics **378**, 686–707 (2019)
[23] Scholand, N., Wang, X., Roeloffs, V., Rosenzweig, S., Uecker, M.: Quantitative mri by nonlinear inversion of the bloch equations. Magnetic Resonance in Medicine (2023)
[24] Song, P., Eldar, Y.C., Mazor, G., Rodrigues, M.R.: Hydra: Hybrid deep magnetic resonance fingerprinting. Medical physics **46**(11), 4951–4969 (2019)
[25] Wang, Z., Li, H., Zhang, Q., Yuan, J., Wang, X.: Magnetic resonance fingerprinting with compressed sensing and distance metric learning. Neurocomputing **174**, 560–570 (2016)
[26] Weigel, M.: Extended phase graphs: dephasing, rf pulses, and echoes-pure and simple. Journal of Magnetic Resonance Imaging **41**(2), 266–295 (2015)
[27] Yang, M., Jiang, Y., Ma, D., Mehta, B.B., Griswold, M.A.: Game of learning bloch equation simulations for mr fingerprinting. arXiv preprint arXiv:2004.02270 (2020)
[28] Yang, Q., Lin, Y., Wang, J., Bao, J., Wang, X., Ma, L., Zhou, Z., Yang, Q., Cai, S., He, H., et al.: Model-based synthetic data-driven learning (most-dl): Application in single-shot t2 mapping with severe head motion using overlapping-echo acquisition. IEEE Transactions on Medical Imaging (2022)
[29] Yang, Y., Sun, J., Li, H., Xu, Z.: Admm-csnet: A deep learning approach for image compressive sensing. IEEE transactions on pattern analysis and machine intelligence **42**(3), 521–538 (2018)